Materials Research Proceedings **4** (2018) 91-96 doi: http://dx.doi.org/10.21741/9781945291678-14

# Fast Temporal and Spatial Resolved Stress Analysis at Laser Surface Line Hardening of Steel AISI 4140

D. Kiefer[1,a*], J. Gibmeier[1,b] and F. Beckmann[2,c]

[1]Karlsruhe Institute of Technology (KIT), Institute for Applied Materials (IAM-WK), Engelbert-Arnold-Str. 4, 76131 Karlsruhe, Germany

[2]Institute of Materials Research, Helmholtz-Zentrum Geesthacht (HZG), Max-Planck-Str. 1, 21502 Geesthacht, Germany

[a]Dominik.Kiefer@kit.edu, [b]Jens.Gibmeier@kit.edu, [c]Felix.Beckmann@hzg.de

**Keywords:** Laser Hardening, X-ray Diffraction, Synchrotron Radiation, Real Time Stress Analysis

**Abstract.** Local and temporal strain and stress evolution is recorded by synchrotron X-ray diffraction during laser line hardening of SAE 4140 steel in the quenched and tempered states at different measuring positions with respect to the process zone. The in-situ diffraction experiments were performed at beamline P05@Petra III at DESY, Hamburg (Germany). The steel samples were line hardened using a 4 kW high-power diode laser (HPDL) unit at a constant laser feed of 800 mm/min. Using a specially designed process chamber that incorporates symmetrically attached fast silicon micro-strip line detectors, stress analysis using the $\sin^2\psi$-method in single-exposure mode, enabled measuring rates at 20 Hz. As a result of the temporal and spatial resolved analyses, the elastic strains were separated from the thermal strains.

## Introduction

In the last decades, with the development of high power diode lasers (HPDL), laser surface hardening gained increased interest for the provision of localized fatigue and wear resistant surface regions of technical components. The process is characterized by localised heat input using a laser beam, followed by self-quenching. Using fiber coupled laser optics the hardening process is rather flexible. Hence, typical applications for structural components are, inter alia, cutting edges, turbine blades or forging matrices that are locally tailored hardened martensite to the application requirements. By this means beneficial residual stress (RS) states can be locally induced in the near surface region that impedes e.g. failure through crack initiation. The advantages over competing surface hardening processes are high automation capability, fast processing and minimal distortion due to the local heat input. However, process prediction is very complex and mainly based on case studies in the final state for the particular material [1-4]. We demonstrated in previous studies that in-situ X-ray diffraction experiments are a suitable tool to investigate fast running thermal and thermo-chemical processes such as laser surface hardening. Here, quick time resolutions require high X-ray photon flux, which can only be provided by synchrotron sources. Results of in-situ diffraction studies during processing help deepen the process understanding and can be used to improve and validate process simulation and thereby allow accurate process predictions. The adaption of the single exposure technique [5] into an experimental setup for laser surface hardening as presented in [6, 7] allows for the real-time monitoring of phase transitions and strain evolutions. Here, a specially designed process chamber was commissioned with measuring and evaluation strategies established that allows for the separation of thermal and elastic strains for each exposure. Finally the stresses were calculated according to the well-known $\sin^2\psi$-method [5]. This set-up was developed further. Earlier work [6] started exclusively with spot hardening experiments. We equipped the process chamber with a motorised tilt holder for the laser

Materials Research Proceedings **4** (2018) 91-96 doi: http://dx.doi.org/10.21741/9781945291678-14

optics that allows for defined laser line hardening experiments. Additionally we established new laser optics with an in-line single color pyrometer that provides fully temperature-controlled processing during laser line hardening. The process chamber, described in [6], was upgraded with more suitable linear motors to provide laser feed speeds on a technically relevant scale. Here, we report about new results that were recorded using this upgraded set-up and about the achievements reached. The results of temporal and spatial resolved phase-, strain- and stress-evolution are discussed.

**Experimental**

Material and sample preparation: For the laser line hardening experiments cuboid samples ($80 \times 50 \times 15$ mm$^3$) made from AISI 4140 steel in a quenched and tempered state were mechanically ground for improved surface smoothness to increase laser absorption and to guarantee a consistent surface quality. Subsequent, the samples were subjected to a stress relief heat treatment at 510°C for 90 min under inert gas atmosphere.

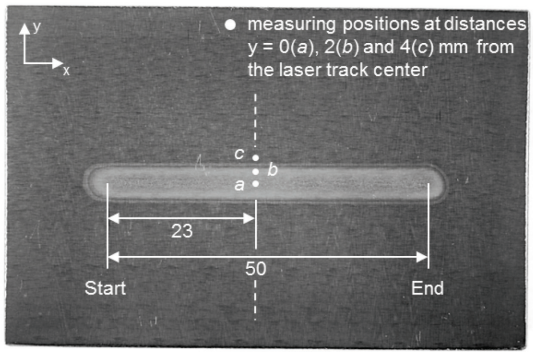


*Fig. 1: Image of laser line hardened sample with the different measuring positions, which were set at 23 mm from the start for the in-situ experiment.*

Experimental setup and implementation: In-situ X-ray diffraction laser line hardening experiments were carried out at the beamline P05@PETRA III operated by the Helmholtz Center Geesthacht (HZG) at DESY in Hamburg, Germany. Synchrotron radiation was provided by a double crystal monochromator and set to E = 10.899 keV (λ = 1.1384 Å). Laser feed speed was set to 800 mm/min from the starting position at a temperature $T_{max}$ = 1150 °C. The laser system comprised a fiber coupled 4 kW high power diode laser unit type LDM 4000-100 in combination with Gaussian focusing optics with a nominal focal point diameter of 5.8 mm: Both from Laserline GmbH, Mühlheim-Kärlich (Germany). Tracks with a length of 50 mm and a nominal width of approx. 5 mm were laser hardened. The X-ray synchrotron investigations were done with a double cross slit that adjusted the X-ray spot size to about $1 \times 1$ mm$^2$. Measurements were taken at three different positions *a*, *b* and *c* that corresponded to distances 0, 2 and 4 mm to the center of the laser track axis as illustrated in Fig. 1. The atmosphere inside the process chamber is set to a low He overpressure to avoid oxide scale formation during the process. The sample is pre-tilted, with respect to the primary beam axis, by an angle $\chi$ = -35°. Key components of the setup are fast micro-strip detectors (MYTHEN-1K, Dectris Ltd.), which are radially (r = 200 mm) arranged around the process chamber in a manner that correspond to the single exposure technique described in [4]. The measuring frequency was set to 20 Hz ($t_{exposure}$ = 50 ms). At the given wavelength both detectors cover a 2θ range of about 140° - 157°. A scheme of the experimental setup is shown in Fig. 2. The setup allows for the simultaneous measurement of a diffraction peak *hkl* from the identical diffraction cone under two different tilt angles $\psi_1$ and $\psi_2$. By definition, ψ is the angle between the sample surface normal $P_3$ and the diffraction vector $N_i^{\{hkl\}}$.

Data processing and analysis: For the detector calibration, powder samples of $LaB_6$ and α-Fe were used. Prior to peak fitting an absorption correction and a linear background subtraction were performed. The diffraction peaks are fitted using a Pseudo-Voigt function. Error bars were calculated on the basis of a 95 % confidence interval for the peak fits. At the chosen synchrotron radiation wavelength the {422} α-Fe ($2\theta_0$ = 153.206°) and the {600} γ-Fe ($2\theta_0$ = 138.790°) peaks

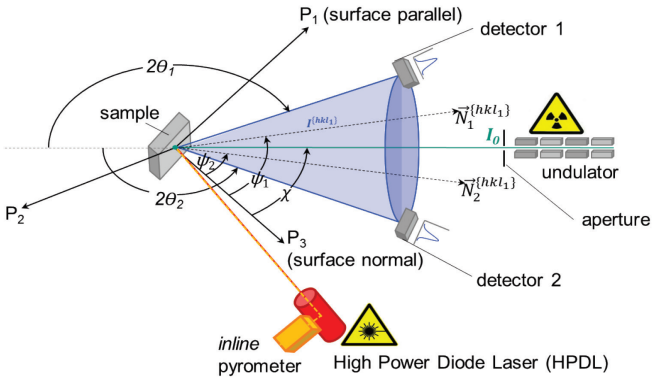


*Fig. 2: Scheme of the experimental in-situ setup with diffraction cone and indicated angles.*

were measured. Thermal strains result in a vertical shift of the 2θ-sin$^2$ψ line plot due to the influence on the hydrostatic part of the stress tensor. On the other hand, elastic strains result in a change of slope. A separation of thermal and elastic strains was performed as described in [6] and the deviatoric stress evolution during the process calculated. Here we focus on the determination of the strain / stress components transverse to the laser track (= transverse to the feed direction). The stress independent lattice directions were calculated from the phase-specific, temperature dependent macroscopic Young's moduli *E* and Poisson ratio *v*.

Post-process investigations: The results of the in-situ stress analyses were compared to high spatially resolved RS lab analyses according to the classical sin$^2$ ψ -method. 41 positions were measured over the laser treated line with an increment step width Δy = 0.25 mm. The measurements were performed using a ψ-diffractometer and V-filtered Cr$K_\alpha$- radiation. Here, the {211} α-Fe diffraction line ($2\theta_0$ = 156.394°) was measured at 13 ψ angles for -60° < ψ < 60°. The primary beam was collimated using a 100 µm focusing polycapillary optics. On the secondary side a 4 mm symmetrical slit was used in front of the scintillation counter.

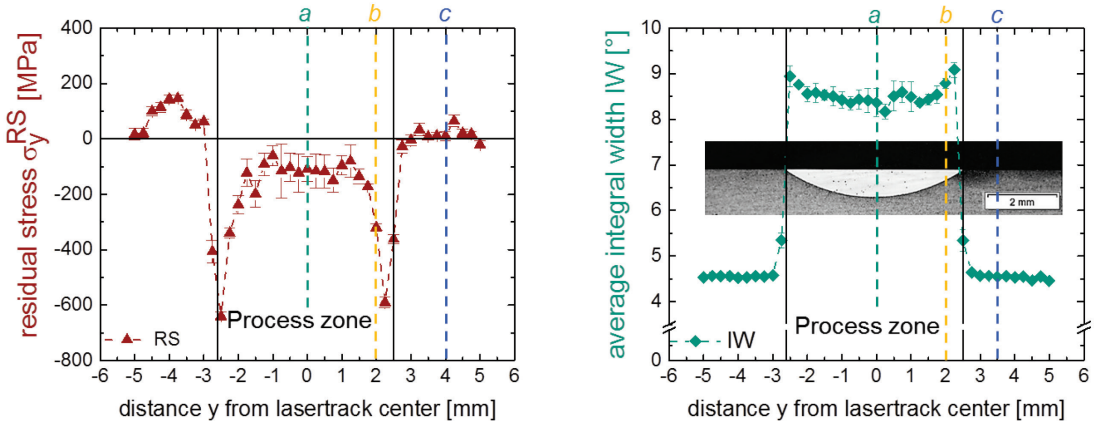


*Fig 3: Results of high resolution RS (transverse component) lab measurements (ex-situ) across the laser track (left) and corresponding average integral peak width of the diffraction lines (right). The in-situ (synchrotron) measuring positions a, b and c is represented by the dashed lines on the two graphs. Also shown (right) is a cross-sectional micrograph of the hardened zone.*

**Results and discussion**

A metallographically prepared cross section of a laser line hardened sample shows an ideally sectorial martensitic hardened zone with a maximum width of 5.1 mm at the surface and a maximum depth of 0.81 mm in the center (see Fig. 3 background). Using a confocal 3D microscope, the surface topography was analyzed post-process showing a peak in the center of the laser track of about 4.3 µm in height compared to the not hardened surface. The results of the high spatially resolved lab measurements (ex-situ study) are plotted in Fig. 3 (left: RS | right: integral peak widths of the diffraction lines).

Transverse residual stresses at the surface show a characteristic W-shaped distribution over the

Materials Research Proceedings **4** (2018) 91-96 doi: http://dx.doi.org/10.21741/9781945291678-14

width of the laser hardened track with a relatively small compressive RS plateau at about -100 MPa in the central section of the laser track. The transition zone is characterized by high compressive RS down to -600 MPa. Outside of the processed area the compressive RS are balanced by tensile RS. The decrease of the compressive RS in the center line of the track is due to a material distortion by volume expansion during martensite formation, i.e. the material flows evades towards the free surface and shows a deformation in this zone. The integral peak widths (see Fig. 3, right) are around 8.5° inside and 4.5° outside the process zone with a steep rise at the edges. This strong line broadening inside the laser treated region is a clear indication of increased dislocation density due to martensitic hardening.

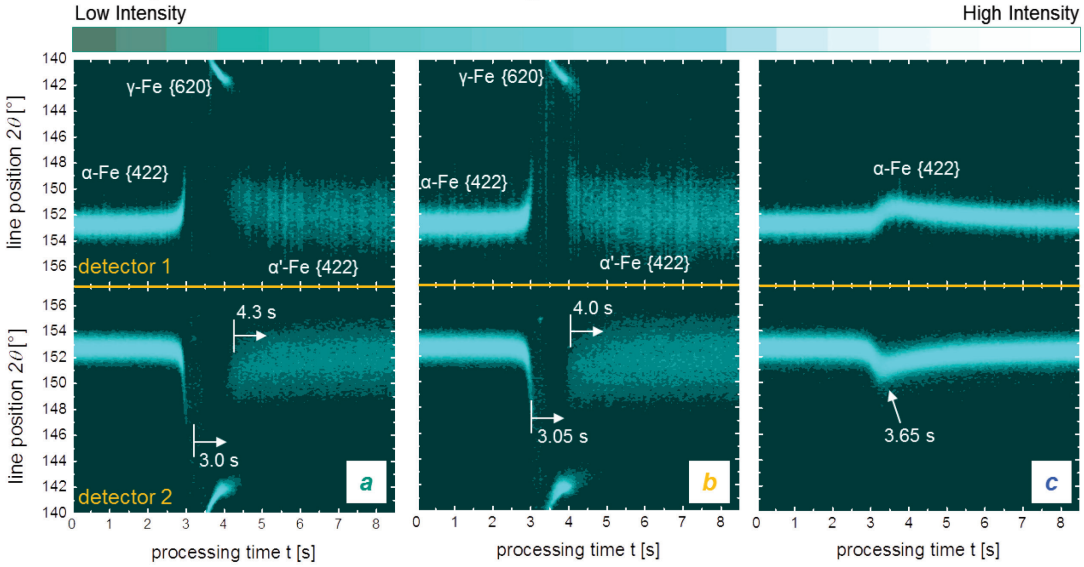


*Fig 4: Normalized X-ray intensity plots recorded during the simultaneous in-situ diffraction analyses and laser hardening treatment. Shown are the results of detectors 1 and 2 at the three different measuring points y = 0 mm (left), 2 mm (middle) and 4 mm (right) of laser track (Fig. 1.). Reflections hkl are indexed in the upper detector 1 plots and the processing timings in the lower detector 2 plots.*

In Fig. 4 normalized X-ray intensity plots recorded during the in-situ synchrotron X-ray diffraction studies that were taken simultaneously with the laser hardening treatment are presented for the three different measuring positions. At approx. 2.8 s a steep and high peak shift for the α-Fe {422} reflection occurs at the measuring positions *a* and *b* (left and middle), followed by the diffraction signal of supercooled {620} γ-Fe at around 3.7 s shifting to higher 2θ values due to increased supercooling up to 4.3 s (left) and 4.0 s (middle) when martensite formation starts. This is characterised by the appearance of the rather broad diffraction lines. The earlier martensite formation for position *b* (at 4.0 s, middle), compared to position *a* (4.3 s, left), can be attributed to the increased cooling rate due to higher degree of self-quenching towards the laser track edge. Outside the laser track at position *c* (Fig. 4, right) no phase transformation occurred. The maximum peak-shift and thus maximum temperature is reached at about 3.65 s. In contrast, at the given feed, the laser beam passes the 23 mm measuring point at 3.3 s. This time delay is a consequence of the time for heat conduction to occur. In Fig. 5 the thermal strains and deviatoric stresses are plotted versus the processing time for the three different measuring positions. The processing temperature $T_{max}$ is plotted next to the thermal strain results. Additionally, results of the ex-situ RS measurements (see Fig. 3) are plotted next to the deviatoric stresses. Maximum thermal strain inside the process zone (positions *a* and *b*) for the heating of ferrite is reached directly before austenite formation starts. Due to the laser heat input that shows a Gaussian function for the

Materials Research Proceedings **4** (2018) 91-96 doi: http://dx.doi.org/10.21741/9781945291678-14

applied optics, the thermal strain is highest in the center of the laser track at 3.1 s when austenisation starts in the process zone. Outside the process zone (position *c*) the maximum thermal strain is delayed to 3.65 s and 3 to 5 times lower than in the process zone which is in good correlation with Fig. 4. With the onset of the martensite formation the thermal strain for position *b* decreases earlier and more rapidly (see Fig. 4) than for position *a.* This is a direct result of the higher local temperature gradient and thereby cooling rate at the edge of the process zone. The lowest cooling occurs at position *c* due to temperature balancing by heat conduction. Considering the stress-time plots for all three positions *a* - *c,* the initial stresses of about -40 MPa show a slight shift towards the tensile regime at e.g. about 2.8 s (position *a*), followed by a sharp decline towards high compressive stresses up to an approximate maximum of -600 MPa (position *b*) at about 3.05 s. The first increase can be explained by a global heating effect, which is almost identical for all three measuring positions. The later drop to high compressive stresses is a consequence of high thermal expansion and the restraint, which are different for the three measuring positions. The compressive stress decrease at measuring position *c,* after reaching a maximum of approximately -400 MPa at about 3.15 s, is assumed to be related with austenite undercooling in the adjacent process zone. The high rate of volume contraction in the process zone during cooling combined with the requirement of material cohesion leads to small tensile stresses, which slightly decrease with the onset of martensite formation in the adjacent process zone to a near stress-free state (at about 4 s). The temporal stress development in the process zone (martensite formation) shows a decrease from about 100 MPa (≈ 4.3 s) to approx. -100 MPa (≈ 9 s) for measuring position *a,* which remains almost constant afterwards. Considering the thermal strain evolution in and outside the process zone, the decrease is a result of decreasing thermal strains. For measuring position *b* the stresses evolve to higher compressive residual stresses of about -300 MPa. This is much steeper than for position *a* due to the fact that volume expansion is locally more constrained. Since martensite formation starts at the edge and develops towards the center of the process zone and temperature is highest in the center, it is assumed that the material deforms plastically in the process zone. However, due to transient temperature distribution, the center is subjected to higher temperatures for a longer time interval that may cause local recovery, resulting in decreased integral widths compared to the edge of the process zone (see Fig. 3 left). The measured material

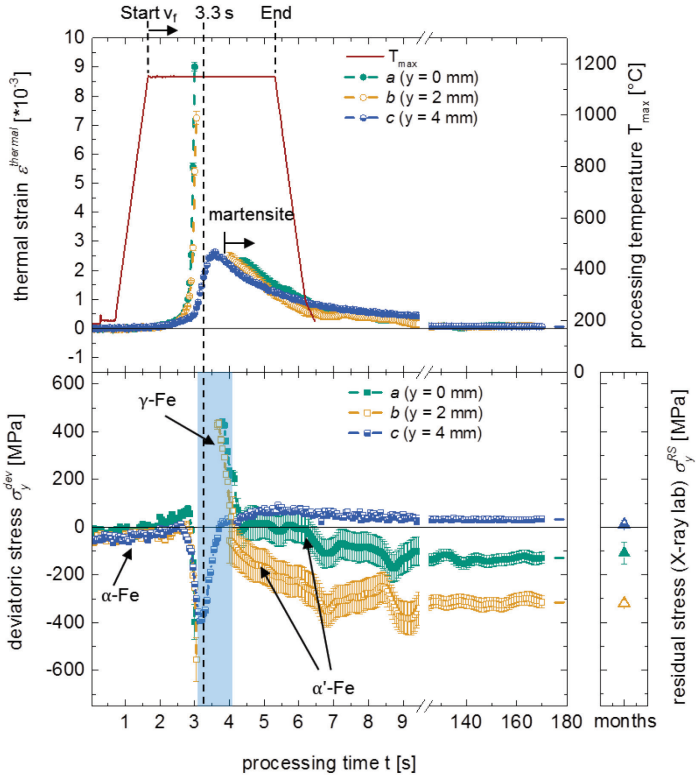


*Fig 5: Thermal strain (top) and deviatoric (bottom) stress (transverse component) evolution during the laser line hardening process for the different measuring positions a, b and c. RS results according to Fig. 3 (bottom left). Light blue background indicates the austenite regime.*

deformation of the process zone supports this point. For all measuring positions at the end of the in-situ determined stresses, the values match well with the results of the RS lab measurements.
In comparison to previous work [6] no significant increase of the surface RS in the center of the laser track was measured. Main reason is the inhomogeneous (Gaussian) energy distribution of the laser beam optics and hence strong differences of local temperature, temperature gradients and cooling rate inside the process zone. The local and transient transformation behaviour may lead to higher degree of transformation plasticity in the track center and hence in lower compressive RS.

## Conclusions

Spatial and time resolved synchrotron X-ray diffraction analysis during laser surface line hardening was successfully carried out. An improved experimental setup (two axes tiltable laser optics with in-line pyrometer) allowed for complete temperature controlled laser hardening processing with feed rates in line with industrial applications.

- Post processing stress measurements are in good agreement with ex-situ lab RS analyses.
- Thermal strain evolution is maximised in the center of the laser track decreasing towards the edge of the hardened zone due to Gaussian power distribution and corresponding heat input.
- Time of martensite formation depends on the position perpendicular to the track axis. Towards the laser track center the lower cooling gradient leads to later martensite formation.
- Local and transient martensite transformation in combination with local material deformation results in lower compressive RS in the track center that increases towards the edge of the process zone.
- Higher strain constraint at the edge of the process zone leads to increased plastic deformation and higher compressive RS compared to the center.

## Acknowledgements

Financial Support by the German Research Foundation (DFG) in the projects GI376/10-1 and BE5341/1-1 is gratefully acknowledged.

## References

[1] T. Miokovic, V. Schulze, O. Vöhringer and D. Löhe, Auswirkung zyklischer Temperaturänderungen beim Laserstrahlhärten auf den Randschichtzustand von vergütetem 42CrMo4, HTM 60 (2005) 142-149. https://doi.org/10.3139/105.100334

[2] K. Obergfell, V. Schulze and O. Vöhringer, Simulation of Phase Transformations and Temperature Profiles by Temperature Controlled Laser Hardening: Influence of Properties of Base Material, Surf. Eng. 19 (2003) 359-363. https://doi.org/10.1179/026708403225007572

[3] K. Müller and H.W. Bergmann, Suitability of materials for laser beam surface hardening, Z. Metallkunde, 90 (1999) 881-887.

[4] P. De la Cruz, M. Odén and T. Ericsson, Effect of laser hardening on the fatigue strength and fracture of a B–Mn steel, Int. J. Fatigue 20 (1998) 389-398. https://doi.org/10.1016/S0142-1123(98)00010-3

[5] E. Macherauch and P. Müller, Das $\sin^2\psi$-Verfahren der röntgenographischen Spannungsermittlung, Z. angew. Phys. 13 (1961) 305-312.

[6] D. Kiefer, J. Gibmeier, F. Beckmann and F. Wilde, In-situ Monitoring of Laser Surface Line Hardening by Means of Synchrotron X-Ray Diffraction, Mat. Res. Proc. 2 (2016) 467-472.

[7] V. Kostov, J. Gibmeier, F. Wilde, P. Staron, R. Rössler and A. Wanner, Fast in situ phase and stress analysis during laser surface treatment: A synchrotron x-ray diffraction approach, Rev. Sci. Instrum. 83(11510) (2012) 1-11. https://doi.org/10.1063/1.4764532